2014 5th IEEE RAS & EMBS International Conference on
Biomedical Robotics and Biomechatronics (BioRob)
August 12-15, 2014. São Paulo, Brazil

Design, characterization and stability test of a Multistable Composite Compliant Actuator for Exoskeletons

Leonardo Cappello[1], Xavier Lachenal[2], Alberto Pirrera[2], Filippo Mattioni[3], Paul M. Weaver[2] and Lorenzo Masia[4]

***Abstract*— A novel actuator is presented that merges traditional electromechanical motors and multistable composite structures. Previously, it has been shown that these structures are able to arrange themselves in multiple stable configurations corresponding to local minima of their strain energy. When coupled with an electromechanical motor as proposed in this article, the resulting actuator shows significant benefits. These are in terms of safety, energy saving and control implementation using the compliance of the overall structure, the particular shape of the strain energy landscape, and the accurately predictable non-linear behavior. Hence the proposed actuator is well-suited for robotics applications. The parameters characterizing the design of the transmission are analyzed, and a physical model is developed. A case study is presented in which the performance for a particular configuration of the system is evaluated and reported. A conceptual application of the proposed actuator is discussed for assistive robotics, where new perspectives on the use of non-rigid transmission elements might become beneficial in terms of safety and energy harvesting.**

Keywords - Multistable Composite Material, Actuator, Assistive Technology, Force and Admittance Control, Z-width.

I. INTRODUCTION

Compliant components are seldom used in robotics applications. This is mostly due to the difficulties related to the design of structurally non-linear flexible parts, and to the consequent computational burden of the control algorithm. Such difficulties and the loss of the inherent high-stiffness are mainly avoided in robotics engineering. Designs are usually based on the use of rigid links and transmission elements, in order to prevent unstable behaviors and unpredictable failures.

Another crucial issue is related to the implementation of robust control architectures for flexible components. To this day, this topic remains to be investigated and presents many open questions, making classical, non-flexible, robotics a more reliable and performing choice.

That said, the literature offers several examples of compliant actuation for robotic applications [1-3]. The disciplines that require compliance in actuation and manipulation are those devoted to human-robot interaction, robotic rehabilitation, haptics and all of the related applications where safety, limitation/filtering of peak forces, and gentle interaction are paramount. The use of compliant parts was proposed in the 90s with the so-called Series Elastic Actuators (SEAs) [4,5], where elastic components were placed between the electromechanical actuators and the load to be manipulated. SEAs present several advantages. However, the compliance introduced by the elastic transmission represents a limitation in applications where accuracy in positioning and repeatability are crucial (i.e. production lines).

In biomimetics, SEAs, as well as Variable Stiffness Actuators (VSA), result in a higher and subtler regulation of the interaction force at the end effector [6,7], because the contact force with the external environment is directly perceived by the linear deformation of the compliant elements and solved as a positioning problem by a linear PID controller [8]. It is worth highlighting that elastic-type non-linearities in hardware components are not necessarily detrimental, especially if we are able to model and predict the resulting dynamic behavior. Previous work by some of the authors focused on modelling of the non-linear static and dynamic response of Multistable Composite Structures (MPSs) [11-13]. These models can be used to design and to implement efficient control algorithms for robotic devices that include MPSs and exploit their inherent compliance.

In the present paper we introduce a novel concept of actuation based on carbon fiber structures, which behave in a nonlinear manner [9]. The proposed architecture consists of a traditional electromechanical actuator, coupled to a novel composite transmission [9,10]; the latter element features nonlinear stiffness characteristics that provide compliance at the end effector. In contrast to the linear elastic elements used in SEAs and VAS, this structure is able to settle into multiple stable configurations over its operative range of motion.

The proposed architecture allows the actuator to attain accurate force and position control, and to overcome the robotics' precept of using stiff components in order to avoid uncontrollable nonlinear dynamics. In fact, the design possibilities offered by composite materials make the proposed multistable transmission predictable and well-controlled over a wide range of deformations.

Following the system stability tests done by the authors in [9], this papers details the design criteria for the multistable transmission. The model is then characterized following a method based on the Z-width procedure [14]. Lastly, some

[1]L. Cappello is with the Robotics Brain and Cognitive Sciences Department, Italian Institute Technology, Genova, Italy Leonardo.Cappello@iit.it

[2]X. Lachenal, [2]A. Pirrera, and [2]P. M. Weaver are with the Advanced Composites Centre for Innovation and Science, University of Bristol, Bristol, UK Xavier.Lachenal@bristol.ac.uk, Alberto.Pirrera@bristol.ac.uk, Paul.Weaver@bristol.ac.uk

[3]F. Mattioni is with Hengshen Carbon Fibre, Southampton, UK Filippo.Mattioni@hscarbonfibre.co.uk

[4]L. Masia is with the Robotic Research Center, School of Mechanical & Aerospace Engineering, Nanyang Technological University, Singapore Lorenzo.Masia@ntu.edu.sg

978-1-4799-3127-9/6/14/$31.00 ©2014 IEEE

potential applications are discussed.

II. OVERVIEW OF THE SYSTEM

A. Synopsis

The proposed solution incorporates a brushless motor and a multistable composite transmission (MCT) (Figure 1) connected to the motor's shaft and devoted to delivering motion to the load. The MCT is made of two pre-stressed flanges of carbon fiber held together by stiff connecting spokes. The MCT is able to take any twisted configuration between a coiled and a straight shape. When the motor shaft rotates one end of the MCT, while the other end is constrained to translate, the structure twists assuming a helical shape that depends on the motor's rotation. The torque delivered by the motor is then transformed into an axial force. The reduction ratio depends on the pitch of the helicoidal configuration of the flanges [9]. The following sections cover an analytical formulation for the MCT's strain energy and the analysis of the MCT's equilibria for specific design parameters.

B. Definitions

The word layup refers to the arrangement of the layers (plies) of composite material that constitute a laminate. It is expressed as a series of numbers between brackets, defining the fibers orientation with respect to a reference axis, e.g. $[\alpha/\beta/\gamma/.../\psi/\omega]$, where Greek letters indicate the fiber angle. A lay-up is said to be symmetric when layers with identical properties, thickness and ply angle are positioned symmetrically with respect to the mid-plane of the laminate [14,15], e.g. $[\alpha/\beta/\chi/\chi/\beta/\alpha]$. Conversely, an anti-symmetric lay-up is defined as $[\alpha/\beta/\chi/-\chi/-\beta/-\alpha]$.

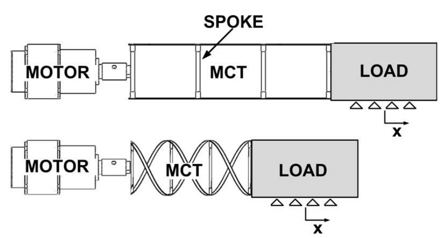

Fig. 1. assembly of the DC motor, the multistable composite transmission and the load.

C. Introduction to system modeling

As previously mentioned, the MCT presents multiple configuration of stability. This means that the structure's strain energy landscape has multiple maxima and minima over the range of permissible rotations (twist angle). The number of peaks (maxima) and valleys (minima), that correspond to points of unstable and stable equilibrium respectively, depends upon several design parameters such as layup, material properties, geometry, and pre-stress of the flanges [10]. In particular, the state of pre-stress simply results from the manufacturing process, because the flanges are manufactured on a cylindrical mold of radius R_i and then assembled in a

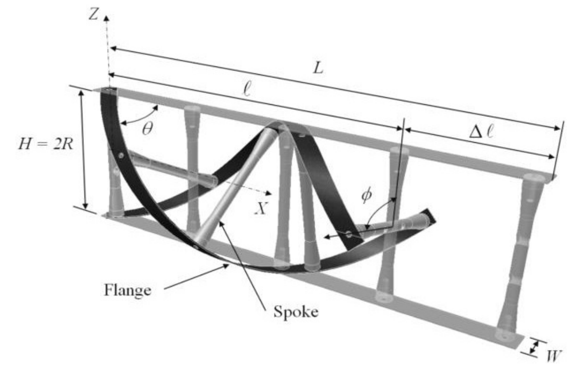

Fig. 2. Sketch showing the structure in the straight (light grey) and twisted (black) configurations. The angle of helix θ and the constant height H of the structure are also shown.

helicoidal structure of radius R. The mechanical behavior of the resulting composite structure is characterized using its strain energy. Note that the rigid spokes keep the flanges at a constant distance throughout the twisting action and it is assumed that the flanges lie tangential to an imaginary underlying cylinder of constant diameter, equal to the spoke's length, $H = 2R$ (Figure 2). Furthermore, because the flanges are narrow, it is assumed that their mid-surface does not stretch and deforms uniformly in bending. Doing so is equivalent to neglecting the stretching component of strain energy associated with the twist of the MCT. These assumptions allow only two parameters to define every possible configurations of the structure: the curvature 1/R of the underlying cylinder, and the pitch θ of the flanges, as illustrated in Figure 2.

D. Strain energy and stable equilibriums

As the transformations are assumed to be inextensional (no stretching) and the curvatures constant over the length and width of the flanges, the strain energy of each flange can be expressed as [15]:

$$U = \frac{1}{2}\Delta\kappa^T D^* \Delta\kappa LW \tag{1}$$

where L, W are the length and width of the flange, respectively. The superscript T denotes the transpose of the vector $\Delta\kappa$ representing changes of curvature (equation (3)), and $D^* = D - BA - 1B$ is the reduced flexural stiffness of the flange as defined in classic lamination theory [16]. In order to find stable configurations, we look for points meeting the following two conditions. The first derivative of the strain energy with respect to the twist angle θ is equal to zero, and the second derivative of the strain energy with respect to θ is strictly positive (point of minimum):

$$\frac{\partial U}{\partial \theta} = 0, \quad \frac{\partial^2 U}{\partial \theta^2} > 0. \tag{2}$$

E. Curvature change

The tensor $\Delta\kappa$ describing the change of curvature can be found for any R and θ in the (x,y) coordinate system, i.e. the local axes attached to each flange (where x is oriented in the longitudinal direction), using a Mohr's circle of curvature [17]. In our case, the parts being manufactured on a curved tool of radius R_i, the initial curvature $\kappa_x = 1/R_i$ must be considered in the expression of the change of curvature; thus the ratio $\alpha = R_i/R$ relating the manufacturing radius R_i and the radius R of the underlying cylinder is defined. It is worth noting that the change of curvature across the width of the flange is not imposed by the geometry of the helix; instead it results from Poisson's ratio effects and is found by solving the equation of moment of the flange about the y-axis considering its free-edge boundary condition. Hence, the change in curvature to any configuration of a flange can be described by the vector $\Delta\kappa$ defined as:

$$\begin{bmatrix}\Delta\kappa_x\\ \Delta\kappa_y\\ \Delta\kappa_z\end{bmatrix} = \frac{1}{2R}\begin{bmatrix} 1-\cos(2\theta)-\frac{2}{\alpha} \\ \frac{D^*_{12}}{D^*_{22}}(\cos(2\theta)+\frac{2}{\alpha}-1)-2\frac{D^*_{26}}{D^*_{22}}\sin(2\theta) \\ 2\sin(2\theta)\end{bmatrix} \tag{3}$$

F. Axial force and twist moment

Applying Castigliano's theorem to the MCT, the axial force, stiffness, twist moment and torsional stiffness can be derived from equation (1), yielding:

$$F = \frac{\partial U}{\partial \Delta\ell}, \quad k = \frac{\partial^2 U}{\partial \Delta\ell^2} \tag{4}$$

$$M = \frac{\partial U}{\partial \phi}, \quad \Gamma = \frac{\partial^2 U}{\partial \phi^2} \tag{5}$$

where F, M are the axial force and twist moment applied to one end of the MCT, respectively; k, Γ are the axial stiffness and torsional stiffness of the MCT, respectively, and $\Delta\ell$ and ϕ are shown in Figure 2.

III. DESIGN PARAMETERS

It should be emphasized that the capability of designing and tuning the proposed transmission is crucial to obtaining a wide range of dynamic and kinematic behaviors to meet different stability and force/torque transmission requirements. These properties play a primary role in making MCTs preferable to traditional stiff transmissions.

The main parameters that allow tailoring the behavior of MCTs are:

- the layup,
- the ratio α between the manufacturing radius R_i and R,
- the length L of the unwrapped flanges,
- the radius R of the underlying cylinder, and
- the width W of the flanges.

A. Effect of the lay-up

The composite layup of the flanges plays a primary role in defining the shape of the transmission's strain energy landscape and thus the corresponding axial force and twist moment that can be delivered to the load as function of the rotational configuration of the MCT. In the present paper we analyze two layups: one symmetric and one anti-symmetric, with stacking sequence $[\beta/\beta/0/\beta/\beta]$ and $[\beta/\beta/0/-\beta/-\beta]$, respectively. The 0° plies in the mid layer of each layup ensures a minimum strength and avoids delamination issues. Five layers are used to ensure a significant strain energy variation during structural deformation, using the material properties given in table I. The influence of β on the strain

TABLE I
CFRP PROPERTIES [18].

Material	E_{11} [GPa]	E_{22} [GPa]	G_{12} [GPa]	ν_{12} [-]	ν_{21} [-]	t [mm]
8552/IM7	164	12	5	0.3	0.022	0.11*

*measured

energy of the system (equation 1) can be described through three-dimensional polar representations and contour plots like those shown in figure 3. In those plots, the radial axis represents the ply axis β and the circumferential axis corresponds to the helix angle θ. Note that β ranges from 0° to 180° to cover the entire range of fiber orientations, whereas θ varies in the range $-\pi < 2\theta < \pi$. This is because, as depicted in figure 2, the structure cannot physically compenetrate and can deform within values of helix inclination comprised in the interval $\theta \in [-\pi/2, \pi/2]$. In addition to figure 3, the

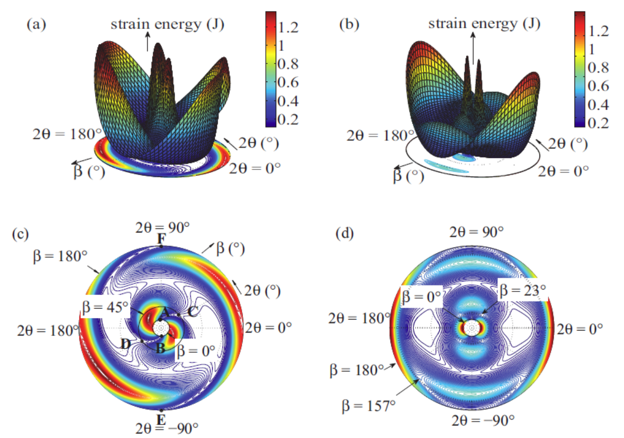

Fig. 3. (a) Surface representation and corresponding contour polar plot of U as a function of 2θ and β for a structure made of a symmetric lay-up $[\beta/\beta/0/\beta/\beta]$, with a ratio $\alpha = 2$ and b ranging from 0° to 180°. High levels of strain energy correspond to unstable configurations of the structure, whereas stable equilibria are found at the lowest levels. (b) Surface representation and corresponding contour polar plot of U as a function of 2θ and β for a structure made of an anti-symmetric lay-up $[\beta/\beta/0/-\beta/-\beta]$, with a ratio $\alpha = 2$ and β ranging from 0° to 180°. (c) Plan view of the polar plot of figure 3a. The dotted lines show the path of the stable equilibria as β increases. The points A, . . . , E correspond to stable positions for specific configurations β =0°, 45° and 180°. (d) Plan view of the polar plot of figure 3b. The dotted straight lines denote stable equilibria. The dotted circles denote a constant strain energy level.

influence of β on the strain energy, twisting torque and axial force are depicted in figure 4a, 4b and 4c respectively for particular values of β. It can be noted that, depending on β, a symmetric layup can generate different sinusoid-like strain energy functions of θ. The slope of these functions changes with β and different slopes mean that the system assumes different stiffnesses upon deformation. Furthermore, the positions of the minima shift as β changes. The meaning of this feature is in the different configuration of equilibrium

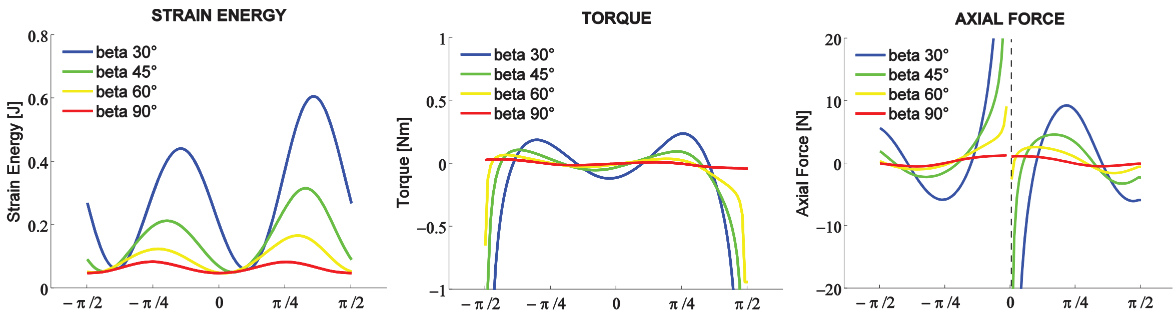

Fig. 4. (a): plot of strain energy U ,(b): plot of twist torque T and (c): plot of axial force F as function of θ and β for a MCT made of a symmetric lay-up up $[\beta/\beta/0/\beta/\beta]$ with $\alpha = 2$, $L = 180$ mm, $R = 27.4$ mm, $W = 10$ mm.

that the system assumes. A final consideration should be made about the amplitude of the strain energy function, which is linked to the input (torque or axial force) required to force the structure into the alternative stable equilibrium. This is easily understood observing the blue and red curves in figure 4b and 4c, where the peak torque/force are much higher for $\beta = 30^\circ$ than $\beta = 90^\circ$.

B. Ratio α

The parameter that regulates the pre-stress of the multistable structure is the ratio α, between the radius of the cylinder from which the carbon strips are manufactured (R_i) and the half-length (R) of the spokes which rigidly connect them. Figure 5 shows the influence of α on the strain energy. It can be observed that the position of the energy's valleys and peaks for a symmetric layup $[45^\circ/45^\circ/0/45^\circ/45^\circ]$ is almost preserved, but their magnitude changes considerably.

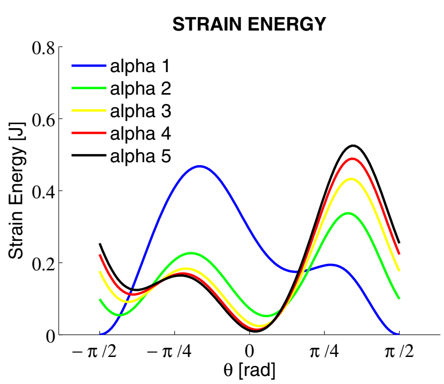

Fig. 5. 2D plot of strain energy U as function of θ and α for a MCT made of a symmetric lay-up up $[45^\circ/45^\circ/0/45^\circ/45^\circ]$ with $L = 180$ mm, $R = 27.4$ mm, $W = 10$ mm.

C. Geometry of the helix

The overall dimensions of the actuator, and hence of the composite transmission, are a crucial design specification. The MCT's dimensions depend on the radius of the helices (R) and its length (L). In this study, the influence if these parameters on the structure strain energy is assessed keeping their ratio constant, as per the following equation:

$$\frac{R}{L} = \frac{1}{\alpha\pi} \tag{6}$$

The effect of different combinations of L and R is reported in figure 6, where it can be seen that longer flanges and larger radii (black line) cause the transmission to be more compliant. It is understood (from figure 2) that the latter case will also lead to larger overall extensions in the MCT's longitudinal direction.

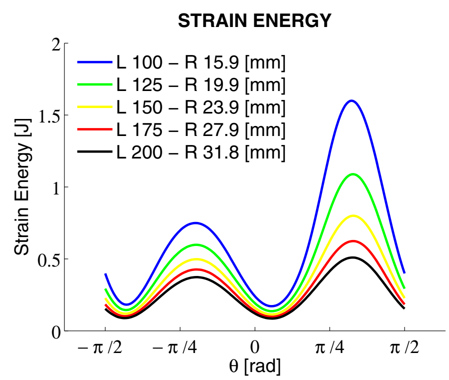

Fig. 6. 2D plot of strain energy U as function of θ and the pair R and L for a MCT made of a symmetric lay-up up $[45^\circ/45^\circ/0/45^\circ/45^\circ]$ with $\alpha = 2$, $W = 10$ mm.

IV. CHARACTERIZATION AND STABILITY TEST

For our experimental setup we chose a MCT with the parameters reported in table II. This section describes the characterization of the stability performance of the admittance controller by testing the limit of the gains. Our test bench includes a brushless motor (Maxon ECi 40 70W and 28:1 gearhead) connected to the MCT and equipped by a uniaxial force sensor (Futek LCM300 100lb capacity) as shown on figure 7. In order to test the system in closed loop, an admittance control scheme was implemented (Figure 8, upper portion), consisting of two nested loops: the outer loop (the force provided by the sensor) is converted by a target admittance block which specifies the desired behavior of the

TABLE II
MCT'S PARAMETERS

Lay-Up	β	α	R	L	W
symmetric	45^o	2	27.4 mm	180 mm	10 mm

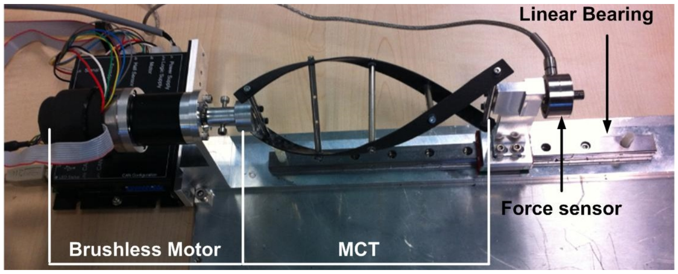

Fig. 7. overview of the test bench, comprising the motor, the MCT and the load cell shifting over a linear bearing.

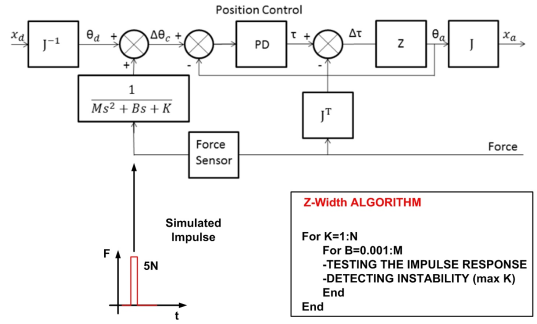

Fig. 8. admittance control scheme of the device and graphical representation of the force impulses used for determining the Z-width of the system. The algorithm for determining the range of achievable impedances is reported.

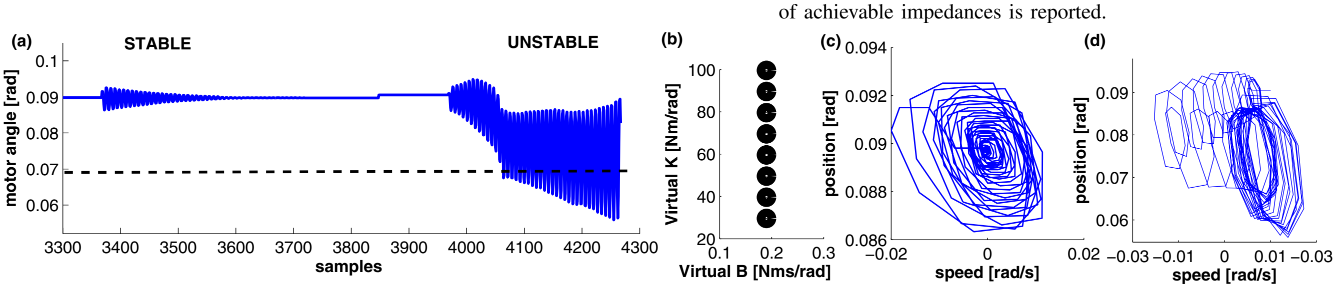

Fig. 9. (a): trajectory of the motion of the motor shaft registered by encoder for either a stable or an unstable oscillatory response. (b): virtual stiffness and virtual damping values input in the controller (c): Phase plot of a stable response. (d): Phase plot of an unstable response.

actuator at the interface with the environment into a desired motion. The target admittance reflects the haptic rendering by the generation of a desired device position. The inner loop is a PD position controller and is used to input the desired generated trajectory. By modifying the parameter M (mass), B (damping), K (stiffness) of the target admittance it is possible to simulate different dynamic response to perturbation. Such parameters represent the simulated mass, damping and stiffness of the system according to the general equation of motion. For our test we chose to simulate a 1 Kg mass system and to gradually vary the damping B and stiffness K of the admittance block to define the range of stability. Since the envisioned application for the actuator is to provide assistance in human robot interaction by displaying position commands after reading interaction forces feedback by the sensor, safety requirement must be accurately fulfill and the range of stability carefully evaluated. A specific performance evaluation for haptic displays can be achieved by determining the Z-width - i.e. the dynamic range of achievable impedances at the end effector [14]. It is important to find the combinations of K and B preserving the system stability. To identify the dynamic range of the system, we tested values of K and B according to the algorithm of figure 8. Starting from a stable configuration of the system, corresponding to a point of local minima for the strain energy, a predetermined displacement X_d is imposed in order to shift the system away from the strain energy valley - i.e. the stable configuration. A simulated force impulse (Figure 8 lower portion) is input to the target admittance block and the consequent simulated trajectory is sent to the PD controller. The response of the system was then observed: if stability is preserved (figure 9b), then a higher K is set in the controller and another step input simulated, until an unstable response arises as observed from the divergent shape of trajectory in figure 9a. At this point the value of K is reset to the lowest and a higher B value is set, gradually increasing K until instability occurs again. An example of stable/unstable response is shown in figure 9c and 9d respectively using the phase plane, where both angular rotation and speed combination are depicted: if the response results in a second order stable oscillation gradually approaching to zero, the phase plane depicts a shape confined in a circular area. On the contrary, a divergent oscillation always results in a phase plane taking an asymmetric shape asymptotically drifting towards a stationary velocity, as depicted in figure 9 d. The tendency of the unstable oscillations to shift the system in the direction of a stable configuration of the MCT, as noticeable from figure 9a, is a remarkable effect.

V. EXPERIMENTAL RESULTS

The described method allowed collecting data of the dynamic range of achievable impedances of the actuator. Data are reported on figure 10. The introduction of the MCT in the actuation stage clearly provides a wider stability range. This is mainly due to the additional intrinsic damping and stiffness of the multistable composite structure, which limit the oscillations for high values of the controller gains and prevents the divergent behavior in case of instability (as observed in figure 9a). It is worth noting that in case of unstable behavior, the system oscillates towards an intrinsically stable strain energy minimum. Therefore, the upper limits for

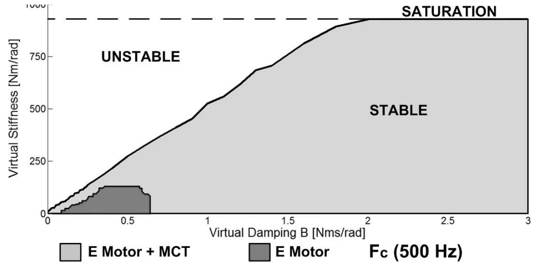

Fig. 10. Z-width of the system composed by the motor and the MCT (grey area) compared with the z-width of the sole electromechanical actuator (dark gray area). The frequency of the control loop used for our tests is reported in the plot.

virtual stiffness and damping are due to the saturation of the actuator for high values of the controller's gains, as depicted in figure 10 by the plateau of the stability curve.

VI. CONCLUSIONS AND OUTLOOK

In this paper we introduced a novel actuator based on conventional technologies like EC motors, and unconventional ones like multistable composite structures. This particular architecture allows us to exploit their respective characteristic features for benefits in several robotics applications. Among them, we mentioned assistive robotics as the field, which may benefit more. According to the assumption adopted by SEAs that elastic elements at the end effector can improve safety in human-interacting robots by filtering disturbances, the proposed actuator can be seen as an alternative/ affordable way to address the same issue. There are several advantages in using multistable composite materials, including their low weight and tailorable dynamic behavior, which make them a competitive alternative to traditional stiff robotics and SEAs. Furthermore, their behavior can be modeled so that, in turn, high levels of control accuracy can be achieved. The authors' aim is to use the proposed actuator to realize a novel assistive exoskeleton (figure 11) whose features are:

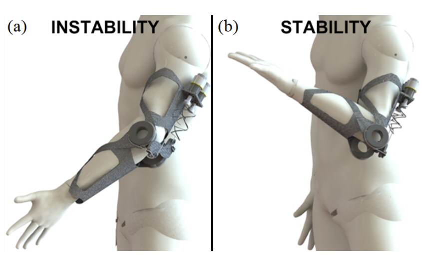

Fig. 11. Conceptual design of an exoskeleton powered by the MCT system. (a): The system is in an unstable configuration in order to harvest energy by exploiting the inertial oscillations of the arm while the user is walking for example. (b): The system is in a stable configuration and the position is held solely by the MCT; thus the motor can be deactivated in order to save energy.

- To save/harvest energy by exploiting the unstable configurations of the MCT during inertial motions in which stability is not required - i.e. the natural oscillation of the arms during the gait - then to adsorb and consequently feedback them;
- To provide assistance in a discrete manner, which means to determine flexion/extension and angular displacements corresponding to stable configurations of the MCT and use motor power only to position the system in a stable state (strain energy valley); once the system is so configured the motor can be switched off, saving large amounts of energy.

A concept design can be seen on figure 11, where a lightweight exoskeleton is worn by a user in two different configurations corresponding to the two features described above.

REFERENCES

[1] De Luca, W. Book, "Robots with Flexible Elements", in Springer Handbook of Robotics, B. Siciliano, O. Khatib (Eds.), pp. 287-317, Springer Verlag, Berlin, 2008.
[2] A. De Luca, P. Lucibello, "A general algorithm for dynamic feedback linearization of robots with elastic joints," 1998 IEEE International Conference on Robotics and Automation, Leuven, B, 1998.
[3] A. Albu-Schaffer, Ch. Ott, and G. Hirzinger, "A unified passivity based control framework for position, torque and impedance control of flexible joint robots", The Int. J. of Robotics Research, vol. 26, no. 1, pp. 23-39, 2007.
[4] G. A. Pratt and M.M. Williamson, "Series Elastic Actuators, Intelligent Robots and Systems", Human Robot Interaction and Cooperative Robots, 1995.
[5] G. A. Pratt and M. M. Williamson, "Series elastic actuators", in Proc.IEEE Int. Workshop on Intelligent Robots and Systems (IROS?95), Pittsburg, USA, 1995, pp. 399-406.
[6] A. D. Luca, F. Flacco, A. Bicchi, and R. Schiavi, "Nonlinear decoupled motion-stiffness control and collision detection/reaction for the vsa-ii variable stiffness device", in IEEE Int. Conf. on Intelligent Robotic Systems, 2009.
[7] S. Haddadin, A. Albu-Schaffer, and G. Hirzinger, "Safety evaluation of physical human-robot interaction via crash-testing", in Robotics: Science and Systems Conference (RSS2007), 2007.
[8] N. Paine, S. Oh, and L. Sentis, "Design and Control Considerations for High-Performance Series Elastic Actuators", IEEE/ASME Trans. Mechatronics, pp. 1-12, 2013.
[9] L. Masia, L. Cappello, P. Morasso, X. Lachenal, A. Pirrera, P. Weaver, and F. Mattioni, "CARAPACE: A novel composite advanced robotic actuator powering assistive compliant exoskeleton preliminary design", IEEE Int. Conf. Rehabil. Robot., vol. 2013, Jun. 2013.
[10] X. Lachenal, P. M. Weaver, S. Daynes. "Multistable composite twisting structure for morphing applications". Proceedings of the Royal Society A: Mathematical, Physical and Engineering Science 2012; 468: 21. DOI: 10.1098/rspa.2011.0631.
[11] A. Pirrera "Bistable Structures for Morphing Applications Using Anisotropic Shells", 2011. Thesis University of Bristol.
[12] A. Pirrera, D. Avitabile, P. M. Weaver "Bistable plates for morphing structures: A refined analytical approach with high-order polynomials", International Journal of Solids and Structures, 47, 2010.
[13] A. Pirrera, D. Avitabile, P. M. Weaver "On the thermally induced bistability of composite cylindrical shells for morphing structures", International Journal of Solids and Structures, 49 (5), 2012.
[14] J. E. Colgate and J. M. Brown, "Factors affecting the Z-Width of a haptic display", Proc. 1994 IEEE Int. Conf. Robot. Autom., no. May, pp. 3205-3210, 1994.
[15] Kollar L. P., Springer G. S., "Mechanics of composite structures". Cambridge, UK: 2003
[16] Jones R. M., "Mechanics of composite materials". 2nd Edn ed.: London, UK: 1999.
[17] Calladine C. R., "Theory of shell structures". Cambridge, UK: 1983.
[18] Hexcel, HexPly 8552 data sheet, 2007, Hexcel.